Research Square

Preprints are preliminary reports that have not undergone peer review.
They should not be considered conclusive, used to inform clinical practice,
or referenced by the media as validated information.

A CDs-doped europium-MOF for ratiometric fluorescence and colorimetric dual-mode sensing of flumequine

Jintao Yi

yistarthappy@163.com

Gannan Normal University

Anqi Li

Gannan Normal University

Xianqin Han

Gannan Normal University

Nani Fu

Gannan Normal University

Ziluo Chen

Gannan Normal University

Tingting Yang

Gannan Normal University

Zihan Zhou

Gannan Normal University

Min Wang

Gannan Normal University

Yashan Chen

Gannan Normal University

Jun Xue

Gannan Normal University

Xiaoming Ma

Gannan Normal University

Yiping Qian

Gannan Normal University

Research Article

Keywords: Flumequine, Eu-2MIM@CDs, Fluorescence, Colorimetric

Posted Date: July 24th, 2026

DOI: https://doi.org/10.21203/rs.3.rs-10372481/v1

License: This work is licensed under a Creative Commons Attribution 4.0 International License.
Read Full License

Additional Declarations: No competing interests reported.

Version of Record: A version of this preprint was published at Microchimica Acta on October 30th, 2026. See the published version at https://doi.org/10.1007/s00604-026-08484-8.

Abstract

Flumequine (FLU), a widely used fluoroquinolone antibiotic, poses serious health risks due to its residual presence in food and the environment, creating a pressing need for on-site visual detection methods. Herein, a dual-mode detection of FLU was achieved using an Eu-2MIM@CDs probe, which was prepared by embedding carbon dots (CDs) into a porous metal–organic framework (Eu-2MIM) composed of europium and 2-methylimidazole. In colorimetric mode, the Eu-2MIM@CDs complex reacted with chromium black T (EBT) to form a magenta Eu^{3+}–EBT complex. Upon the introduction of FLU, FLU competitively displaced EBT from the complex, releasing free EBT and restoring the blue color. This displacement process was accompanied by ratiometric absorbance changes at 538 nm and 610 nm, enabling multi-color visual detection. In fluorescence mode, the Eu-2MIM@CDs probe initially exhibited emission from CDs at 436 nm. Upon adding FLU, the antenna effect sensitized Eu^{3+}, which simultaneously quenched the emission at 436 nm and generated a new emission peak at 612 nm, yielding a concentration-dependent ratiometric fluorescence response for FLU detection. In colorimetric mode, as the FLU concentration increased, the absorbance at 538 nm progressively decreased while that at 610 nm increased, producing a well-defined ratiometric colorimetric signal. This mode provided a wide linear detection range from 0.01 to 2.5 μM with a detection limit of 3.3 nM. The visible color of the solution shifted from magenta to blue with rising FLU concentration. In fluorescence mode, the intensity at 436 nm gradually decreased along with an increase at 612 nm, showing a linear range from 0.005 to 2.0 μM and a detection limit of 1.7 nM. The fluorescence response was rapid, completing within 1 minute. As the FLU concentration increased, a visible color shifted from blue to red. Both detection modes exhibited excellent selectivity for FLU against various interfering antibiotics, organic compounds and metal ions. Furthermore, the probe showed good practicability in actual samples. Collectively, the dual-mode probe provides a simple, fast and efficient method for both visual and quantitative FLU detection in complex matrices.

Introduction

Flumequine (FLU), a member of the fluoroquinolone family of antibiotics, has been extensively utilized in clinical therapy, livestock farming and aquaculture, due to its broad-spectrum antibacterial activity. However, its overuse and poor biodegradability have resulted in undesirable residues in animal-derived products [1]. These residues can enter the human body through the food chain, leading to adverse effects such as tendon rupture, aortic dissection, and hepatic damage [2]. To mitigate such risks, the European Union has established a maximum residue limit of 10 μg/kg for fluoroquinolones in meat [3]. Consequently, the monitoring of FLU residues has become an imperative task in food safety control. Conventional analytical methods, including high-performance liquid chromatography [4], mass spectrometry [5], and micellar liquid chromatography [6], offer high accuracy. Nevertheless, they suffer from drawbacks including costly instrumentation, tedious sample pretreatment and professional operational requirements, which limit their applicability for rapid on-site detection of flumequine. Therefore, developing simple, cost-effective and field-deployable detection methods for flumequine is of significant importance.

Subsequently, numerous new methods for fluoroquinolones detection have been developed, including phosphorescence sensor array [7], immunochromatographic strips [8], molecularly imprinted polymer method [9]. Phosphorescent sensor arrays offer high sensitivity and multi-target discrimination but suffer from complex preparation, poor stability and environmental interference. Immunochromatographic strips are simple, low-cost and rapid, yet their low sensitivity and susceptibility to operational and matrix effects limit accuracy. Molecularly imprinted polymers provide stable and reusable recognition, but face issues of template leakage, cross-reactivity, tedious synthesis and reduced efficiency in complex samples. Despite these advances, FLU sensing still encounters common challenges: insufficient anti-interference capability in complex matrices, inadequate selectivity against structural analogs, limited trace-level sensitivity, and the difficulty of adapting laboratory methods to rapid on-site analysis. To overcome these drawbacks, ratiometric sensing techniques integrating fluorescence and colorimetry have recently been developed [10, 11]. These methods possess self-calibration capability, which effectively suppresses interferences from environmental factors, instrument fluctuations, and variations in probe concentration, thereby significantly enhancing detection reliability and accuracy. Dual-mode sensors offer both visual qualitative and precise quantitative information, especially beneficial in complex matrices [12, 13]. Ratiometric dual-mode probes enable convenient visual and sensitive quantitative detection, making them well-suited for flumequine analysis.

Metal-organic frameworks (MOFs) are porous crystalline materials with ultrahigh porosity, structural diversity and surface functionality, making them excellent scaffolds for constructing hybrid nanocomposites [14, 15]. By strategically integrating luminescent components such as lanthanide ions or carbon dots (CDs), synergistic materials with enhanced or novel photophysical properties can be engineered [16]. Specifically, lanthanide-based MOFs (Ln-MOFs) exhibit unique luminescent features including long lifetime, large Stokes shift and narrow emission bands, while CDs offer excellent optical tunability, photostability and biocompatibility [17]. In addition to their luminescent capabilities, numerous MOFs have been identified as potent nanozymes, exhibiting a range of enzyme-mimicking activities including oxidase-like, peroxidase-like, protease-like, and nuclease-like properties. Compared with natural enzymes, these MOF-based nanozymes offer distinct advantages, including high selectivity, low cost, robust stability and superior catalytic activity [18, 19]. Consequently, they have been widely employed in visualization sensing using colorimetric methods. Leveraging these exceptional properties, a multimodal detection platform can be constructed for the sensitive detection of flumequine residues.

Herein, a dual-mode detection of FLU was achieved using an Eu-2MIM@CDs probe, which was prepared by embedding CDs into a porous metal-organic framework (Eu-2MIM) composed of europium and 2-methylimidazole. In the colorimetric mode, the Eu-2MIM@CDs probe reacted with eriochrome black T (EBT) to form a magenta Eu^{3+}-EBT complex. Adding FLU displaced EBT from this complex, recovering the blue color of free EBT. This displacement caused ratiometric absorbance shifts at 538 nm and 610 nm, allowing multi-color visual detection of FLU. In the fluorescence mode, the Eu-2MIM@CDs probe emitted at 436 nm from CDs. Adding FLU triggered the antenna effect, which sensitized Eu^{3+}. This process quenched the 436 nm emission and created a new peak at 612 nm, producing a ratiometric fluorescence response that depended on FLU concentration. A paper-based test strip integrated with

smartphone colorimetric analysis was then developed for rapid on-site FLU detection. The developed Eu-2MIM@CDs probe has several advantages: (1) Ratiometric colorimetric/fluorometric sensing enables self-calibration against environmental and instrumental interferences; (2) This dual-mode design combines colorimetric and fluorescent readouts for cross-validated accuracy, on-site screening and high-sensitivity quantification, offering convenient, sensitive and reliable multi-scenario applications; (3) Integration with paper strips and smartphone-based colorimetry supports portable, user-friendly and instrument-free on-site screening, making it well-suited for resource-limited environments. This first Eu-2MIM@CDs-based dual-mode platform for FLU detection holds promise for complex environmental analysis.

Experimental

Reagents and materials

Glucose ($C_6H_{12}O_6$), eriochrome black T (EBT), fetal bovine serum, hydrochloric acid (HCl) and trihydroxymethyl aminomethane (Tris) were purchased from Sangon Biological Engineering Technology (Shanghai, China). Europium (III) chloride hexahydrate ($EuCl_3·6H_2O$), 2-methylimidazole (2-MIM), N, N-dimethylformamide (DMF), manganese chloride ($MnCl_2$), zinc chloride ($ZnCl_2$), melamine (MPF), tryptophane (TRP), benzimidazole (DRB), glucose (GLU), coumarin (CUO) and urea were purchased from Sinopharm Chemical Reagent (Shanghai, China). Flumequine (FLU), amoxicillin (AMO), ampicillin (AMP), cephalotin (CEF), oxacillin sodium (OXA), cephalexin (CEP), vancomycin (VAN), erythromycin (ERY), levofloxacin (LFX), ciprofloxacin (CIP), gatifloxacin (GAT), fleroxacin (FLE), enrofloxacin (ENRO), fusidinic (FUS), sodium penicillin g (PG), oxytetracycline (TCT) and sparfloxacin (SPA) were purchased from Aladdin Reagent (Shanghai, China). Laboratory tap water was used as the environmental water sample. Milk and pork were purchased from a local supermarket near Gannan Normal University. Ultrapure water (resistivity > 18.25 MΩ·cm) was produced by a Millipore Milli-Q water purification system.

Instruments

Scanning electron microscopy (SEM) images were collected using a field-emission SEM (FEI, Holland). Transmission electron microscopy (TEM) was performed on a 2100F field-emission high-resolution transmission electron microscope (Joel, Japan). X-ray diffraction (XRD) patterns were recorded on a D8 Advance diffractometer (Bruker, Germany). Thermogravimetric analysis (TGA) was conducted using a TA Q50 thermal gravimetric analyzer (TA Instruments, USA). Fourier-transform infrared (FT-IR) spectra were obtained on a Nicolet spectrometer (Thermo Fisher, USA). Zeta potential measurements were carried out using a Zetasizer Nano ZS90 (Malvern, UK). UV–visible absorption spectra were recorded on a UV-2700 spectrophotometer (Shimadzu, Japan). Fluorescence spectra were measured with an FS5 fluorescence spectrometer (Edinburgh, UK). High-performance liquid chromatography (HPLC) analysis was performed on an LC-10A system (Shimadzu, Japan).

Synthesis of Eu-2MIM@CDs

Eu-2MIM was synthesized with minor modifications to a reported method [20]. In a 30 mL beaker, a solution of $EuCl_3 \cdot 6H_2O$ (0.015 g/mL) and a solution of 2-MIM (0.0035 g/mL) were combined and ultrasonicated for 10 min. The mixture was then transferred into a Teflon-lined stainless-steel autoclave and heated at 180°C for 12 h. The resulting product was collected by centrifugation at 5000 rpm for 5 min, washed three times with methanol, and dried at 60°C to obtain Eu-2MIM powder. CDs were prepared with slight modifications to a reported method [21]. Glucose (1.0 g), DMF (200 μL) and ultrapure water (30 mL) were mixed and stirred at room temperature for 1 h. The mixture was then heated at 200°C for 24 h. After cooling to room temperature, the mixture was filtered using a bag filter (MWCO 550) for 24 h. The resulting CD dispersion was stored at 4°C for subsequent use. The composite Eu-2MIM@CDs was obtained by mixing Eu-2MIM with the CDs.

Colorimetric and fluorescence detection of FLU

For colorimetric detection of FLU, Eu-2MIM@CDs (0.125 mg/mL) and EBT (0.01 mg/mL) were reacted in Tris–HCl buffer (0.1 M, pH 8) for 1 min. Then, different concentrations of FLU solutions (0 to 2.5 μM) were added and incubated for 10 min. UV–Vis absorption spectra were recorded in the range of 400 to 800 nm. For fluorescence detection of FLU, Eu-2MIM@CDs (0.25 mg/mL) and various concentrations of FLU solutions (0 to 2.25 μM) were mixed at room temperature for 1 min. Fluorescence spectra were collected from 330 to 800 nm with an excitation wavelength of 310 nm. For test-strip visualization, strips were pretreated with Eu-2MIM@CDs solution (0.25 mg/mL). After drying, different concentrations of FLU solutions were applied, and the fluorescence was photographed under UV light.

Actual sample testing

Real sample analysis encompassed four representative matrices: tap water, commercial milk, bovine serum, and pork muscle tissue, pretreating of these samples according to the reference [22]. Water samples were clarified by centrifugation at 8000 rpm for 5 min. Serum samples were pre-filtered through 0.22 μm pore size membranes to remove particulate matter. Milk samples, mixing with acetonitrile, were sonicated and centrifuged to collect the supernatant for analysis. Pork samples (0.2 g) was thoroughly homogenized, extracted with 10 mL of anhydrous ethanol via ultrasonication for 10 minutes, allowed to settle for 2 minutes, and the supernatant was filtered through a 0.22 μm membrane. Finally, a series of FLU solutions at different concentrations were prepared by treated actual samples. In high-performance liquid chromatography (HPLC) analysis, the actual samples were filtered through a 220 nm microporous filter membrane. The mobile phase for FLU detection consisted of acetonitrile and formic acid in a ratio of 15:85. The experimental parameters were set as follows: flow rate of 0.25 mL/min, detection duration of 20 min, detection wavelength of 324 nm for FLU, C18 chromatographic column, and injection volume of 10 μL. The study involving bovine serum was approved by the Ethics Review Committee of Gannan Normal University.

Results and Discussion

Design and detection principle

In this work, as illustrated in **Scheme 1**, a composite material named Eu-2MIM@CDs was constructed by integrating carbon dots (CDs) into the Eu-2MIM framework. The CDs were synthesized using DMF, while the Eu-2MIM framework was composed of europium and 2-MIM. In the colorimetric mode, a magenta Eu^{3+}-EBT complex was formed from Eu-2MIM@CDs and eriochrome black T (EBT). Upon FLU introduction, a competitive displacement occurred, where FLU bound to Eu^{3+} to form a more stable Eu^{3+}-FLU complex and released free EBT, resulting in an observable blue color and ratiometric absorbance shifts at 538 nm and 610 nm. In fluorescence mode, the Eu-2MIM@CDs probe initially exhibited a fluorescence signal at 436 nm under excitation at 310 nm. Upon the addition of FLU, the signal at 436 nm was quenched, while a new signal at 612 nm emerged due to the sensitizing effect of FLU on Eu^{3+}, leading to a ratiometric fluorescence response that varied with increasing FLU concentration. Furthermore, a paper-based test strip combined with smartphone colorimetric analysis was developed for rapid FLU detection on-site.

<**Scheme 1** is here>

Characterization of Eu-2MIM@CDs

Comprehensive characterization revealed the structural and morphological features of the Eu-2MIM@CDs nanocomposites. The Eu-2MIM exhibited rectangular block morphology with smooth surfaces and a uniform size of approximately 4 μm by scanning electron microscopy (SEM) and transmission electron microscopy (TEM) imaging (**Fig. 1A and B**). After CD incorporation, the composite preserved these morphological features without aggregation or deformation (**Fig. 1C and D**), indicating that the Eu-2MIM architecture remained intact. Energy-dispersive X-ray spectroscopy (EDS) mapping revealed homogeneous spatial distribution of C, N, and Eu elements in both Eu-2MIM and Eu-2MIM@CDs (**Fig. S1 and Fig. 1E**), without elemental segregation or phase separation, confirming the uniform incorporation of CDs into the matrix. X-ray diffraction (XRD) analysis further confirmed structural preservation. The Eu-2MIM framework showed characteristic peaks at 10.0°, 15.4°, 20.0°, 32.3°, 40.1°, 45.1°, and 53.9°, and the Eu-2MIM@CQDs composite exhibited nearly identical patterns without new phases or peak broadening (**Fig. 1F**), indicating that the CDs occupied framework interstices or external surfaces without disrupting the coordination bonds maintaining long-range order. Thermogravimetric analysis (TGA) confirmed that both Eu-2MIM and Eu-2MIM@CDs remained stable below 300°C. A pronounced mass loss, originating from the thermal decomposition of organic components, was observed only between 300–380 °C, whereas above 380 °C, both materials retained over 80% of their initial mass as europium oxide residues (**Fig. 1G**). The comparable decomposition profiles indicated that incorporating CDs had little effect on the framework's thermal stability. Fourier transform infrared (FT-IR) analysis showed that the peak at 1620 cm^{-1} originated from C=O stretching, and the bands at 1226-1500 cm^{-1} from C=N and C-N stretching of the heterocyclic ring (**Fig. S2**). The enhanced band width and peak intensity in Eu-2MIM@CDs were attributed to surface groups of CDs, confirming successful synthesis.

ZETA potential analysis revealed that the potential shifted from 13.11 mV for Eu-2MIM to -60 mV for Eu-2MIM@CDs (**Fig. 1H**), a reversal attributed to the abundant negatively charged surface groups of CDs that made the composite negatively charged. Dynamic light scattering (DLS) results showed negligible particle size change after CD incorporation (**Fig. S3**), due to the small size and tight adsorption of CDs onto Eu-2MIM. Taken together, these findings collectively confirmed the successful synthesis of Eu-2MIM@CDs.

<**Figure 1** is here>

Colorimetric Detection of FLU by Eu-2MIM@CDs

The colorimetric detection capability of Eu-2MIM@CDs for FLU was systematically evaluated. As shown in **Fig. 2A**, Eu-2MIM@CDs or FLU alone exhibited no absorption peaks and the solutions remained colorless (curves a□c). In contrast, EBT alone showed a strong absorption peak at 610 nm, with the solution appearing blue (curve b). Upon the coexistence of Eu-2MIM@CDs and EBT, a new absorption peak emerged at 538 nm and the solution turned purplish red (curve d), indicating the complexation between Eu^{3+} and EBT to form Eu^{3+}–EBT complexes. This transformation shifted EBT from its free state to the complexed state, accompanied by a color change from blue to purplish red. When FLU was introduced into the Eu-2MIM@CDs/EBT mixture, the absorbance at 538 nm decreased while that at 610 nm increased significantly, and the solution reverted from purplish red to blue (curve g). This observation suggested that FLU had a stronger complexation affinity toward Eu^{3+} than EBT, thereby displacing EBT from the Eu^{3+}–EBT complex and restoring its free state. Given the distinct color difference between free (blue) and complexed (purplish red) EBT, as well as the FLU concentration-dependent regulation of EBT speciation, the absorbance ratio at 610 nm and 538 nm ($R_{610\ nm/538\ nm}$) could be employed for the ratiometric colorimetric detection of FLU.

To determine the optimal reaction conditions, the effects of pH, EBT concentration, Eu-2MIM@CDs concentration, and reaction time were systematically examined. The $R_{610\ nm/538\ nm}$ ratio was strongly pH-dependent. At pH 2–6, the ratio was low and the solution was orange, whereas at pH 7–11, the ratio increased substantially and the solution turned blue. As both the ratio and color remained stable at pH ≥ 8 (**Fig. S4**), pH 8 was chosen as the optimal pH value. The incubation time was also optimized (**Fig. S5**), which showed that the $R_{610\ nm/538\ nm}$ ratio decreased rapidly and reached a plateau at 7 min. Accordingly, 7 min was selected as the optimal incubation time. The concentrations of EBT and Eu-2MIM@CDs were further optimized. Increasing the EBT concentration led to gradual increases in both the absorbance at 610 nm and the $R_{610\ nm/538\ nm}$ ratio, with the ratio reaching a maximum and stabilizing above 0.011 mg/mL, accompanied by a color transition from light blue to dark blue (**Fig. S6**). Thus, 0.011 mg/mL was adopted as the optimal EBT concentration. Conversely, increasing the Eu-2MIM@CDs concentration resulted in decreased absorbance at 610 nm and increased absorbance at 538 nm, causing the $R_{610\ nm/538\ nm}$ ratio to decline progressively. The ratio reached its minimum and stabilized at 0.275 mg/mL, with the solution color shifting from blue to purplish red (**Fig. S7**). Hence, 0.275 mg/mL was determined as the optimal Eu-2MIM@CDs concentration. In addition, the detection time and stability of the sensing

system for FLU were investigated. The $R_{610\ nm/538\ nm}$ ratio increased with time and peaked at 10 min (**Fig. S8**), which was thus chosen as the optimal reaction time. Afterward, the absorbance values were recorded every 10 min, and the $R_{610\ nm/538\ nm}$ ratio remained stable over 60 min (**Fig. S9**), demonstrating the satisfactory stability of the Eu-2MIM@CDs sensor for FLU detection.

The analytical performance of the Eu-2MIM@CDs sensing platform was evaluated for the colorimetric detection of FLU under the optimized conditions. The ratiometric colorimetric method was employed for the quantitative detection of FLU. In the concentration range of 0–2.5 μM, as the FLU concentration increased, the absorbance at 538 nm decreased while that at 610 nm increased, and the $R_{610\ nm/538\ nm}$ ratio exhibited a good linear relationship with the FLU concentration (**Fig. 2B, C**), accompanied by a gradual color change of the solution from purplish red to blue. The linear regression equation was $R_{610\ nm/538\ nm} = 0.3917C_{FLU} + 0.5105$ ($R^2 = 0.9976$). The limit of detection (LOD) was calculated to be 3.3 nM based on 3δ/slope, which was comparable to those of previously reported nanomaterial-based detection methods (**Table S1** [23-25]). The selectivity and anti-interference performance of the sensor were assessed against four organic compounds (MPF, TRP, DRB, CUO), two metal ions (Mn^{2+} and Zn^{2+}), and thirteen antibiotics (AMO, CEP, AMP, OXA, CEF, VAN, ERY, LFX, CIP, GAT, FLE, ENRO, SPA). As shown in **Fig. 2D**, even at a 5-fold higher concentration than FLU, no significant signal changes were observed for all tested species except for six FLU analogues (LFX, CIP, GAT, FLE, ENRO and SPA), as reflected by low $R_{610\ nm/538\ nm}$ ratios and red color development, confirming the good selectivity for FLU. Notably, the six analogues exhibited comparable responses to FLU (high ratios and blue color), indicating the sensor's capability for detecting FLU analogues. In the presence of coexisting interferents with FLU, the signal responses remained similar to that of FLU alone, with high ratios and blue color (**Fig. 2E**), demonstrating strong anti-interference ability. Therefore, this colorimetric sensor provided a promising platform for highly selective and quantitative FLU detection, with potential applications in diverse fields.

< **Figure 2** is here >

To evaluate the practicality and reproducibility of the proposed sensor, recovery experiments were conducted using real samples. Different concentrations of FLU (0.5, 1.0, 1.5 and 2.0 μM) were spiked into tap water, milk, serum and pork samples for detection. The obtained recoveries ranged from 85.1% to 101.9%, with relative standard deviations (RSDs) between 0.20% and 3.7%, indicating that the ratiometric colorimetric sensor exhibited satisfactory accuracy and reliability. To further validate the method, conventional high-performance liquid chromatography (HPLC) was employed for comparative analysis on the same batch of samples. The HPLC method yielded recoveries of 88.1%–112.0% and RSDs of 0.1%–3.5%, which were comparable to those obtained by the ratiometric colorimetric method (**Table 1**). These results collectively demonstrated that the proposed sensor was accurate and reliable for the determination of FLU in real environmental samples.

< **Table 1** is here >

Fluorescence Detection of FLU by Eu-2MIM@CDs

The sensitization effect of FLU on the Eu-2MIM@CDs sensor was first examined. As shown in **Fig. 3A**, Eu-2MIM@CDs exhibited no distinct absorption peak, whereas FLU showed a maximum at 310 nm. Upon mixing with Eu-2MIM@CDs, the absorbance of FLU at 310 nm increased significantly, confirming the interaction between FLU and the probe. Under excitation at 310 nm, the Eu-2MIM@CDs/FLU system displayed emission bands at 436, 590, 612 and 690 nm (**Fig. 3B**), indicating effective sensitization of Eu^{3+} by FLU. The feasibility of using Eu-2MIM@CDs for FLU detection was then assessed. As presented in **Fig. 3C**, Eu-2MIM@CDs alone exhibited fluorescence at 436 nm (blue line), while FLU alone showed weak emission (green line). In contrast, the Eu-2MIM@CDs/FLU mixture exhibited markedly enhanced emission at 612 nm and quenched emission at 436 nm (purple line), suggesting that FLU can be detected by the ratio probe. The corresponding fluorescence intensity ratio ($R_{612\ nm/436\ nm}$) showed the same trend (**Fig. S10**).

Optimization of Eu-2MIM@CDs concentration and reaction time was performed to establish optimal sensing conditions. As the Eu-2MIM@CDs concentration increased from 0 to 0.275 mg/mL, the fluorescence at 436 nm increased linearly, reached a maximum at 0.275 mg/mL, and then leveled off (**Fig. S11**). Thus, 0.275 mg/mL was chosen as the optimal concentration for further studies. The optimal response time was then investigated, the $R_{612\ nm/436\ nm}$ ratio rose sharply with time and reached a plateau within 1 min (**Fig. S12**). Also, the bar chart of response times confirmed these findings. Therefore, 1 min was selected as the optimal incubation time.

Under optimized conditions, the analytical performance of the Eu-2MIM@CDs probe for FLU detection was systematically evaluated. In the concentration range of 0–2.25 μM, increasing FLU concentrations resulted in a gradual decrease in fluorescence intensity at 436 nm and a concomitant increase at 612 nm (**Fig. 3D**). As shown in **Fig. 3E**, the fluorescence intensity ratio $R_{612\ nm/436\ nm}$ exhibited a good linear relationship with FLU concentration, yielding the calibration equation $R_{612\ nm/436\ nm} = 0.7295\ C_{FLU} + 0.0159$ ($R^2 = 0.9969$). The detection limit was determined to be 1.7 nM based on the 3σ/slope criterion, which was comparable to those of other nanomaterial-based methods **(Table S1** [26-29]). Under UV illumination, a visible color transition from blue to red was observed with increasing FLU concentration (Fig. 3E). This color evolution was further assessed using the Commission Internationale de L'Eclairage (CIE) image (**Fig. 3F**), where the coordinate points shifted from the blue region (FLU, 0 μM) to the red region (FLU, 2.25 μM), confirming the multicolor fluorescence response of the Eu-2MIM@CDs sensor to FLU.

The selectivity and anti-interference performance of the Eu-2MIM@CDs ratiometric sensor for FLU fluorescence detection were evaluated with various potentially interfering species, including three organic compounds (GLU, CUO, UREA), two inorganic ions (Mn^{2+}, Zn^{2+}), and nine antibiotics (SPA, FUS, AMO, CEP, AMP, PG, TCT, VAN, ERY), with SPA being structural analogs of FLU. As shown in **Fig. 3G**, even at five-fold higher concentrations than FLU, only FLU produced a notably high $R_{612\ nm/436\ nm}$ ratio, while all other interferents yielded low ratios, correspondingly, only the FLU-containing solution exhibited red fluorescence, whereas others appeared blue. These results confirmed the high selectivity of the probe

toward FLU. The anti-interference ability was further assessed in **Fig. 3H**, where the co-addition of interferents with FLU maintained high $R_{612\ nm/436\ nm}$ values and red fluorescence, demonstrating robust anti-interference performance. Overall, the developed ratiometric fluorescent sensor provided a promising approach for the specific and accurate detection of FLU, with good applicability in complex sample matrices.

<Figure 3 is here**>**

To elucidate the fluorescence quenching mechanisms of Eu-2MIM@CDs, we investigated the absorption spectra of FLU. A significant spectral overlap was observed between the UV absorption band of FLU and the excitation spectrum of Eu-2MIM@CDs (**Fig. 4A**), implying the presence of an inner filter effect (IFE) that accounted for the fluorescence quenching of Eu-2MIM@CDs upon FLU introduction. As the FLU concentration increased, the UV absorbance intensified progressively, accompanied by the appearance of a new absorption peak (**Fig. 4B**), which pointed to the formation of a complex through the interaction between FLU and the probe. Furthermore, the quinoline ring in FLU, acting as a strong chromophore, facilitated an antenna effect by transferring the absorbed excitation energy to Eu^{3+}, thereby sensitizing Eu^{3+} emission and resulting in a marked enhancement of its characteristic fluorescence. In contrast, other common antibiotics were unable to effectively trigger this antenna effect or achieve energy transfer. Among them, sparfloxacin, although also a quinolone drug, bore substituents such as piperazine on its side chain that created steric hindrance, preventing efficient coordination with Eu^{3+}. Fusidic acid, owing to its steroidal skeleton, lacked a conjugated aromatic system capable of effective coordination with Eu^{3+}. β-Lactam antibiotics, including amoxicillin, cephalexin, ampicillin, and sodium penicillin G, lacked suitable coordinating functional groups. Oxytetracycline, due to its large molecular volume, could not effectively interact with Eu-2MIM@CDs. Erythromycin, with its stable macrocyclic lactone structure and lack of reactive coordinating groups, failed to achieve matched energy transfer. Consequently, none of these structural analogs or other classes of antibiotics could sensitize Eu^{3+} fluorescence through the antenna effect, thereby ensuring the high selectivity of this probe for the detection of flumequine.

<Figure 4 is here**>**

The practical utility of the Eu-2MIM@CDs sensing system for FLU detection was further evaluated through spiked recovery experiments in tap water, milk, serum, and pork samples at three concentration levels (0.5, 1.0, and 1.5 μM). As summarized in **Table 2**, the recovery rates ranged from 81.1% to 106.0% with RSDs of 0.1%–4.5%, indicating satisfactory accuracy and precision. Notably, distinct fluorescence color changes were observed with varying FLU concentrations, facilitating visual identification. The reliability of the proposed method was further validated by HPLC, which yielded recoveries of 88.0%–112.0% with RSDs of 0.1%–3.5%, in good agreement with the results obtained by the ratiometric fluorescence assay. Collectively, these findings demonstrated that the developed method was highly practical and reliable for the determination of FLU in complex environmental matrices.

< **Table 2** is here >

Conclusions

In summary, a novel and sensitive ratiometric dual-mode probe of Eu-2MIM@CDs has been successfully constructed for the efficient detection of FLU. In the colorimetric mode, the absorbance at 538 nm gradually decreased while that at 610 nm increased with increasing FLU concentration, yielding a well-defined ratiometric colorimetric response. This mode exhibited a good linear relationship over the concentration range of 0.01–2.5 μM with a detection limit of 3.3 nM, accompanied by a visible color change of the solution from magenta to blue, enabling naked-eye discrimination. In the fluorescence mode, the emission intensity at 436 nm progressively decreased along with a concomitant increase at 612 nm, showing a linear range of 0.005–2.0 μM and a detection limit as low as 1.7 nM. The fluorescence response was rapid, with the entire assay completed within 1 minute. Meanwhile, a distinct fluorescence color transition from blue to red was clearly observable by the naked eye. Both detection modes exhibited excellent selectivity toward FLU over various interfering antibiotics, organic compounds, and metal ions. Furthermore, the probe demonstrated good practicability in tap water, milk, serum and pork samples, with results highly consistent with those obtained by HPLC method. The proposed Eu-2MIM@CDs-based method shows considerable promise for applications in medication guidance and food safety supervision. Real-time monitoring of antibiotic levels using this probe helps prevent the risks associated with underdosing or overdosing. Its application to veterinary drug residue detection facilitates the management of residual risks, ensures compliance with food safety regulations, and minimizes adverse environmental impacts.

Declarations

Author contributions Jintao Yi: methodology, writing-original draft, funding acquisition. Anqi Li, Xianqin Han, Nani Fu and Ziluo Chen: project administration, data curation. Zihan Zhou, Min Wang and Yashan Chen: software, methodology. Jun Xue: formal analysis. Tingting Yang and Xiaoming Ma: writing-review, funding acquisition. Yiping Qian: writing-review & editing, funding acquisition. All authors have read and agreed to the published version of the manuscript.

Funding This work was supported by Jiangxi Provincial Natural Science Foundation (No. 20242BAB20091), the First Batch of Key University-Level Incubation Projects for the 20th "Challenge Cup" Competition of Gannan Normal University (No. tzb2026017), the Jiangxi Provincial Degree and Graduate Education Teaching Research Reform Project (No. JXYJG-2024-119), the Open Project Program of Key Laboratory of Institute for Quality & Safety and Standards of Agricultural Products Research Jiangxi Academy of Agricultural Sciences (No. KL-KF-202403).

Data availability Data will be made available on request.

Competing interests The authors declare no competing financial interests.

Artificial Intelligence Statement

No artificial intelligence (AI) tools were used in the preparation of this manuscript.

References

1. Jara B, Srain BM, Aranda M, Fernández C, Pantoja-Gutiérrez S, Méjanelle L (2022) Water-sediment partitioning of flumequine and florfenicol, two antibiotics used in salmon aquaculture in Chile. Mar Pollut Bull 177:113480–113487. https://doi.org/10.1016/j.marpolbul.2022.113480
2. Castrignanò E, Yang ZG, Feil EJ, Bade R, Castiglioni S, Causanilles A, Gracia-Lor E, Hernandez F, Plósz BG, Ramin P, Rousis NI, Ryu Y, Thomas KV, Voogt PD, Zuccato E, Kasprzyk-Hordern B (2020) Enantiomeric profiling of quinolones and quinolones resistance gene qnrS in European wastewaters. Water Res 175:115653–115667. https://doi.org/10.1016/j.watres.2020.115653
3. Serrano MJ, Mata L, Pellicer S, Segura-Gil I, Razquin P, Pagán R (2024) Development and validation of a rapid lateral flow test for the detection of fluoroquinolones in meat and blood. Food Control 156:110116–110121. https://doi.org/10.1016/j.foodcont.2023.110116
4. Zhai HY, Liang GH, Guo XJ, Chen ZG, Yu JE, Lin HD, Zhou Q (2019) Novel coordination imprinted polymer monolithic column applied to the solid-phase extraction of flumequine from fish samples. J Chromatogr B 1118:55–62. https://doi.org/10.1016/j.jchromb.2019.04.023
5. Ringenier M, Cherlet M, Dewulf J, Devreese M (2024) Residue depletion of enrofloxacin and flumequine in feathers of broilers based on quantitative UHPLC-MS/MS detection. Food Addit Contam Part A 41:1065–1076. https://doi.org/10.1080/19440049.2024.2370367
6. Peris-Vicente J, Iborra-Millet JJ, Albiol-Chiva J, Carda-Broch S, Esteve-Romero J (2019) A rapid and reliable assay to determine flumequine, marbofloxacin, difloxacin, and sarafloxacin in commonly consumed meat by micellar liquid chromatography. J Sci Food Agric 99:1375–1383. https://doi.org/10.1002/jsfa.9314
7. Wang HG, Zhang BB, Qin YL, Shi YE, Wang YL, Shi SK, Wang ZG (2025) AI one-click-processing-assisted ratiometric RTP paper-based sensor array for the rapid discrimination and detection of mixtures of oxolinic acid and flumequine. Anal Chem 97:22787–22796. https://doi.org/10.1021/acs.analchem.5c04191
8. Liu YX, Jiang K, Li XL, Lu LF, Sun MH, Li N, Madushika L, Yuan J, Ling SM, Wang SH (2025) Development of sensitive and specific immunochromatographic strips with nanoparticles for rapid detection of flumequine. Food Chem X 29:102771–102781. https://doi.org/10.1016/j.fochx.2025.102771
9. Gao K, Jiang MM, Wang M, Dong X, Li JL, Li QJ, Wang FY (2025) Highly sensitive and rapid detection of flumequine in food samples by fluorescent molecularly imprinted microparticles. Microchem J 218:115432–115440. https://doi.org/10.1016/j.microc.2025.115432
10. Chen XR, Tu YJ, Cheng S, Guo XJ, Lu TY, Guo YQ, Huang XL, Xiong YH, Tang BZ (2022) A colorimetric and ratiometric fluorescent paper chip for biogenic amine monitoring based on a simple pH-sensitive AIEgen. Chem Eng J 450:137928–137936. https://doi.org/10.1016/j.cej.2022.137928

11. Ren AS, Qiao LG, Li KC, Zhu DJ, Zhang YZ (2024) Mitochondria-targeted NIR ratiometric and colorimetric fluorescent probe for biothiols based on a thiol-chromene click reaction. Anal Chem 96:17773–17780. https://doi.org/10.1021/acs.analchem.4c04119
12. Huang XY, Yan LX, Zhao X, Lin H, Chen LJ, Yan XP (2026) A ratiometric luminescent nanoprobe based on Eu^{3+}-modified zinc gallogermanate for smartphone-assisted visual detection of tetracycline in food samples. Microchim Acta 193:386–397. https://doi.org/10.1007/s00604-026-08107-2
13. Liang ZG, Yu Y, Chen X, Qin LL, Xu GH, Wei FD, Wang J, Hu Q, Cen Y (2025) Breakthrough in LbCas12a chemical inhibitor screening: The firefly probe and its application in dual-mode biosensors. Anal Chem 97:16050–16057. https://doi.org/10.1021/acs.analchem.5c03437
14. Sun YX, Li ZG, He J, Quan KJ, Qiu HD, Chen J (2026) Regulated zirconium-based metal organic frameworks via ligand-defect and rare earth post-coordination: A synchronized strategy for enhancing Cr (VI) adsorption and phenol photodegradation. Chem Eng J 533:174745–174758. https://doi.org/10.1016/j.cej.2026.174745
15. Wei KJ, He MY, Zhang J, Zhao C, Nie CP, Zhang T, Liu Y, Chen TT, Jiang JH, Chu X (2023) A DNA logic circuit equipped with a biological amplifier loaded into biomimetic ZIF-8 nanoparticles enables accurate identification of specific cancers in vivo. Angew Chem Int Ed 62:e202307025. https://doi.org/10.1002/anie.202307025
16. Zhang HD, Wu SF, Xing ZH, Wang HB (2021) Turning waste into treasure: chicken eggshell membrane derived fluorescent carbon nanodots for the rapid and sensitive detection of Hg^{2+} and glutathione. Analyst 146:7250–7256. https://doi.org/10.1039/d1an01582f
17. Ji Z, Wang HZ, Canossa S, Wuttke S, Yaghi OM (2020) Pore chemistry of metal–organic frameworks. Adv Funct Mater 30:2000238. https://doi.org/10.1002/adfm.202000238
18. Zhou HT, Sun H, Zhang ZB, Fang X, Bu SJ, Li CX, Wan Y, Li N, Hao Z, Ma CY, Lv N, Wan JY (2026) A highly sensitive colorimetric platform based on tricoordinate metal MOFs nanoenzymes and smartphone RGB–assisted analysis for visualized detection of Salmonella typhimurium. Anal Bioanal Chem 418:3211–3226. https://doi.org/10.1007/s00216-026-06424-2
19. Yang Y, Chen XM, Hou DG, Chen YT, Qiu ZL (2026) MOF-on-MOF tandem nanozymes with autonomous substrate transformation for photoelectrochemical and paper-based colorimetric dual-mode aptasensing of neomycin. Microchim Acta 193:153–166. https://doi.org/10.1007/s00604-026-07895-x
20. Yi JT, Han XQ, Jian JH, Lai YY, Lu J, Peng L, Liu ZK, Xue J, Zhou H, Li X (2024) Dual-mode detection of 2,6-pyridinedicarboxylic acid based on the enhanced peroxidase-like activity and fluorescence property of novel Eu-MOFs. Anal Methods 16:2606–2614. https://doi.org/10.1039/d4ay00331d
21. Zhang JH, Wang J, Ouyang FJ, Zheng Z, Huang XW, Zhang HT, He DX, He SS, Wei H, Yu CY (2023) A smartphone-integrated portable platform based on polychromatic ratiometric fluorescent paper sensors for visual quantitative determination of norfloxacin. Anal Chim Acta 1279:341837–341842. https://doi.org/10.1016/j.aca.2023.341837

22. Kong RM, Li PH, Ge XY, Zhao Y, Kong WH, Xiang MH, Xia L, Qu FL (2023) Ratiometric fluorescence determination of alkaline phosphatase activity based on carbon dots and Ce. Microchim Acta 190:487–496. https://doi.org/10.1007/s00604-023-06048-8
23. Liu YX, Jiang K, Li XL, Lu LF, Sun MH, Li N, Madushika L, Yuan J, Ling SM, Wang SH (2025) Development of sensitive and specific immunochromatographic strips with nanoparticles for rapid detection of flumequine. Food Chemistry: X 29:102771–102781. https://doi.org/10.1016/j.fochx.2025.102771
24. Guo SY, Liu M, Liu HL, Mao JR, Zou YF, Sun LP, Huang Y, Sun DD, Ma J (2025) A reflective microfiber biosensor for monitoring of trace flumequine residues enhanced by europium-incorporated covalent organic framework. Microchem J 217:114929–114942. https://doi.org/10.1016/j.microc.2025.114929
25. Ktari N, Fourati N, Zerrouki C, Ruan M, Seydou M, Barbaut F, Nal F, Yaakoubi N, Chehimi MM, Kalfat R (2015) Design of a polypyrrole MIP-SAW sensor for selective detection of flumequine in aqueous media. Correlation between experimental results and DFT calculations. RSC Adv 5:88666–88674. https://doi.org/10.1039/c5ra16237h
26. Jing XQ, Guo MN, Li JR, Xu W, Qin HN, Xiao WD, Wan YH, Chen JL, Yao ZW, Song WJ, Yu HD, Hu K, Li TG (2024) An Eu (III)-functionalized covalent organic framework fluorescent probe for specific detection of Flumequine based on pore restriction and antenna effect. Spectrochim Acta A: Mol Biomol Spectrosc 323:124884–124894. https://doi.org/10.1016/j.saa.2024.124884
27. Zhu K, Fan RQ, Zhang J, Jiang X, Jia WW, Wang BW, Lu HY, Wu JK, Wang P, Yang YL (2021) Dual-emission 3D supramolecular framework hydrogel beads: highly selective detection of antibiotics and mechanism research. Dalton Trans 50:15679–15688. https://doi.org/10.1039/d1dt02733f
28. Yi JT, Fu NN, Li AQ, Yan P, Pan H, Deng XL, Xue J, Li X (2025) Fluorescent determination of flumequine using a novel tryptophan (Trp)—zeolitic imidazolate framework-8 (ZIF-8)—terbium (III) visual probe. Anal Lett 59:1124–1137. https://doi.org/10.1080/00032719.2025.2530052
29. Gao K, Jiang MM, Wang M, Dong X, Li JL, Li QJ, Wang FY (2025) Highly sensitive and rapid detection of flumequine in food samples by fluorescent molecularly imprinted microparticles. Microchem J 218:115432–115440. https://doi.org/10.1016/j.microc.2025.115432

Tables

Table 1 and 2 are available in the Supplementary Files section.

Figures

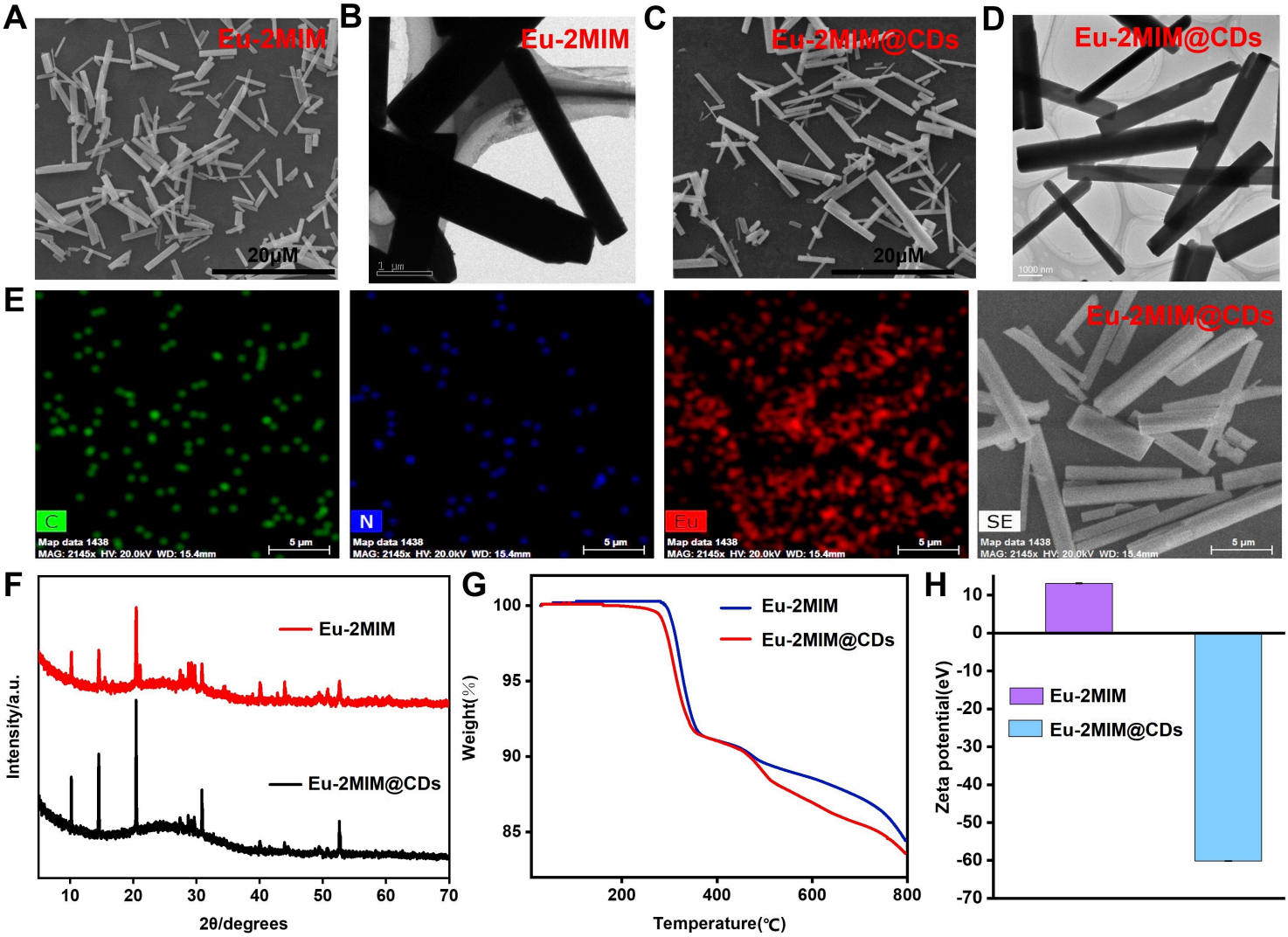


Figure 1

Characterization of Eu-2MIM and Eu-2MIM@CDs. (A) The scanning electron microscope image of Eu-2MIM. Scale bar, 20 μm. (B) The transmission electron microscope image of Eu-2MIM. Scale bar, 1 μm. (C) The scanning electron microscope image of Eu-2MIM@CDs. Scale bar, 20 μm. (D) The transmission electron microscope image of Eu-2MIM@CDs. Scale bar, 1 μm. (E) The elemental mapping images of Eu-2MIM@CDs. Scale bar, 5 μm. (F) The X-ray diffraction patterns. (G) The thermogravimetric analysis. (H) The zeta potential. The error bars represented the standard deviation from three parallel experiments.

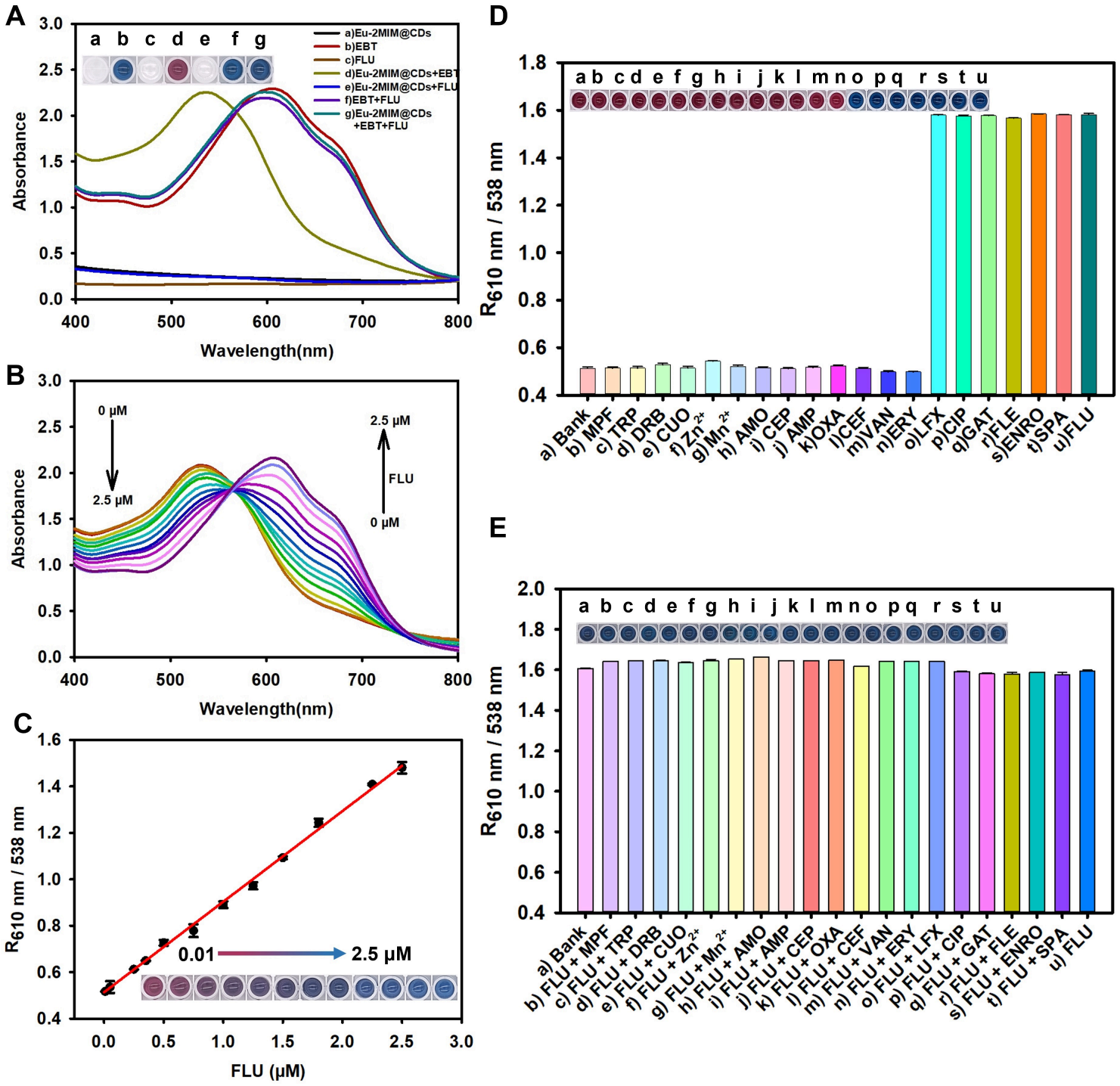


Figure 2

The colorimetric detection of FLU by Eu-2MIM@CDs. (A) The feasibility detection. Inset: the colorimetric images. (B) The UV-vis absorption spectra with different FLU concentrations. (C) The linear relationship between the absorbance ratio $R_{610\ nm/538\ nm}$ and the FLU concentrations, where $R_{610\ nm/538\ nm}$ represented the absorbance value at 610 nm versus that at 538 nm. Insert: the colorimetric images. (D) The selectivity of FLU or interferent. Insert: the colorimetric images. (E) The specificity of FLU and one of interferents. Inset: the colorimetric image. The error bars represented the standard deviation from three parallel experiments.

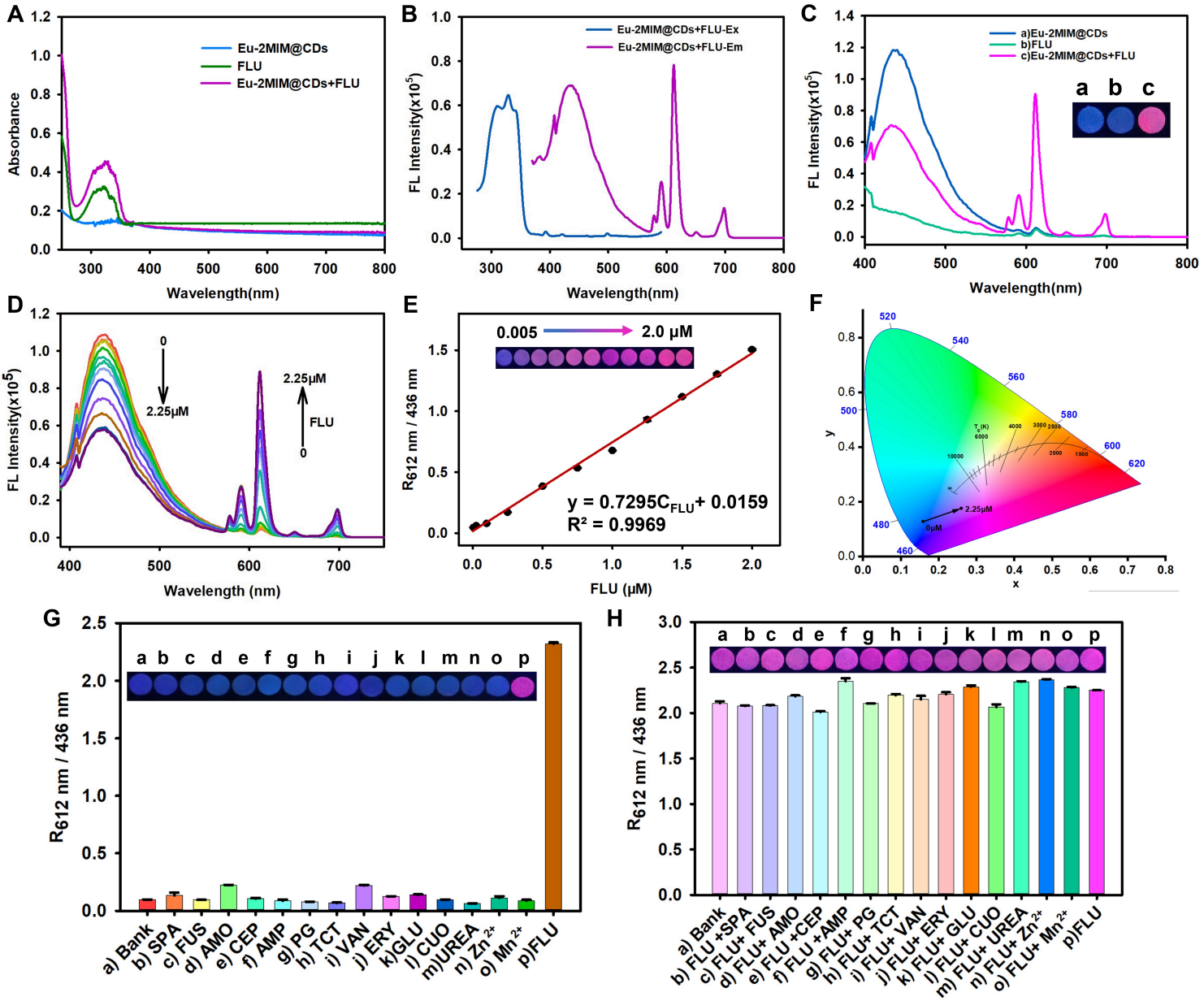


Figure 3

The fluorescence detection of FLU. (A) The UV-vis absorption spectra of Eu-2MIM@CDs, FLU, Eu-2MIM@CDs in the presence of FLU. (B) The excitation and emission spectra of Eu-2MIM@CDs and FLU. (C) The feasibility spectra of Eu-2MIM@CDs, FLU, Eu-2MIM@CDs and FLU. Inset: the fluorescence images. (D) The fluorescence spectra with different FLU concentrations. (E) A linear relationship between the fluorescence intensity ratio $R_{612\ nm/436\ nm}$ and FLU concentrations, where $R_{612\ nm/436\ nm}$ represented the fluorescence intensity value at 612 nm versus that at 436 nm. Inset: the fluorescence images. (F) The corresponding CIE chromaticity coordinates. (G) The selectivity of FLU or interferent. Inset: the fluorescence images. (H) The specificity of FLU and one of interferents. Inset: the fluorescence images. Error bars represented standard deviations from three independent measurements.

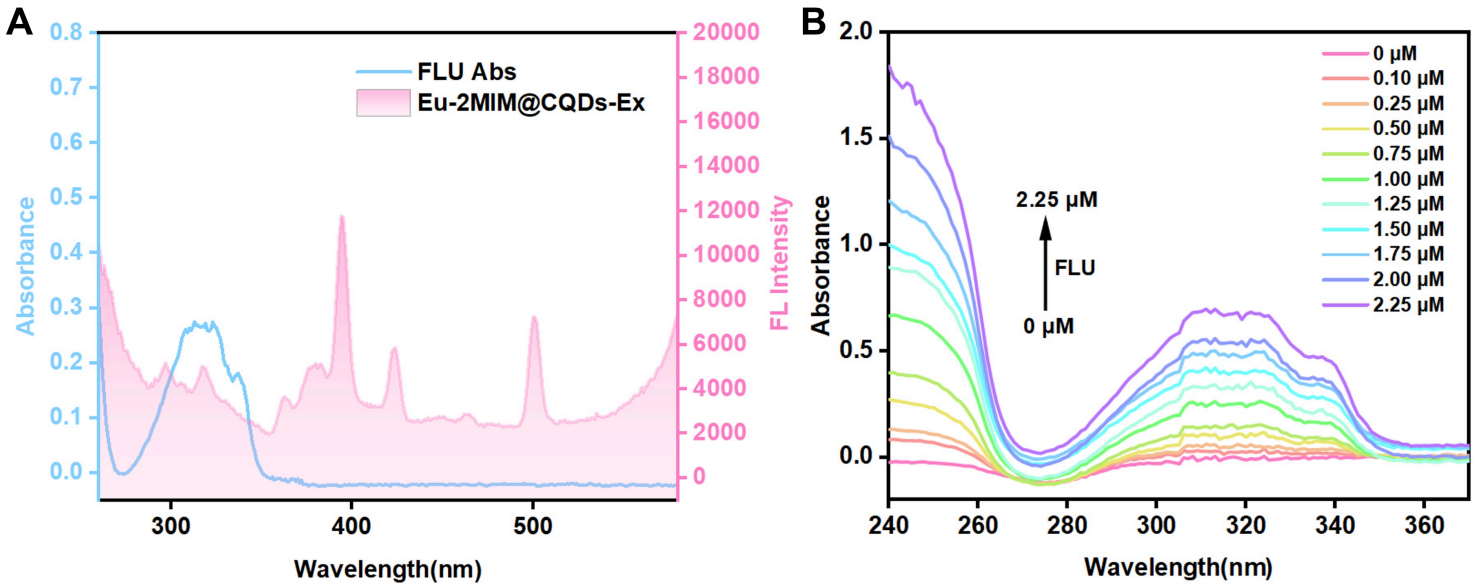


Figure 4

The fluorescence mechanism of FLU detection by Eu-2MIM@CDs. (A) The excitation spectra of Eu-2MIM@CDs. The UV-vis absorption spectra of FLU. (B) The UV-vis absorption spectra of Eu-2MIM@CDs upon addition of different concentrations of FLU.

Supplementary Files

This is a list of supplementary files associated with this preprint. Click to download.

- supportinginformation.docx
- Scheme1.jpg
- TOC.jpg
- Tables.docx